RF Design and Experimental Test of a Quadrupole-Free X-Band TM_{01} Mode Launcher

G. Torrisi*[1]*, G. S. Mauro*[1,2]*,
G. Sorbello*[3,1]*, G. Castorina*[4]*, L. Celona*[1]*,
L. Faillace*[4]*, B. Spataro*[4]*,
***and V. Dolgashev*[5]

[1]Istituto Nazionale di Fisica Nucleare
Laboratori Nazionali del Sud (INFN-LNS)
Via S. Sofia 62, 95123 Catania, Italy
E-mail:giuseppe.torrisi@lns.infn.it

[2]Dipartimento di Ingegneria dell'Informazione,
delle Infrastrutture e dell'Energia Sostenibile
Università degli Studi Mediterranea di Reggio Calabria
Salita Melissari
89124 Reggio Calabria RC

[3]Dipartimento di Ingegneria Elettrica, Elettronica e
Informatica
Università degli Studi di Catania
Viale Andrea Doria 6, 95125, Catania, Italy

[4]Istituto Nazionale di Fisica Nucleare
Laboratori Nazionali di Frascati (INFN-LNF)
Via Enrico Fermi, 40, 00044 Frascati RM Italy

[5]SLAC National Accelerator Laboratory
Menlo Park, USA

Abstract

In this work, we present a low-power RF characterization of a novel TM_{01} X-band mode launcher for the new generation of high-brightness RF photo-injectors. The proposed structure employs a fourfold symmetry in order to minimize both the dipole and the quadrupole fields that could cause an emittance growth in the early stages of the acceleration process. A "cold" model aluminum structure, comprising two mode launchers connected by a central 62 mm-long circular waveguide, was fabricated by milling aluminum blocks, assembled and measured in back-to-back configuration. The low-power RF test, performed at the Istituto Nazionale di Fisica Nucleare Laboratori Nazionali del Sud (INFN-LNS), validated both the numerical simulations and the quality of the fabrication. An oxygen-free high-conductivity copper version of the device is being manufactured for high-power and ultra-high-vacuum tests that are planned to be conducted at the Stanford Linear Accelerator Center (SLAC).

1. Introduction and Motivation

High-gradient radio-frequency (RF) devices will be crucial for innovative accelerating structures to increase brilliance of accelerated bunches. Accelerating gradients up to 250 MV/m can be achieved using cryogenically cooled copper accelerating structures [2, 1]. High brilliance and high field quality are required in the RF photo guns and in its power coupler.

This work presents a novel power coupler, working at X band, which is able to convert the input rectangular TE_{10} mode into a circular TM_{01} mode that can be used for particle acceleration. The device employs a fourfold symmetry in order to minimize the undesired RF components that can arise in the mode-launching section, causing an undesired emittance growth during the first stages of the accelerating process [7]. In particular, the work was focused on the low-power RF tests performed on an aluminum prototype, consisting of two identical mode

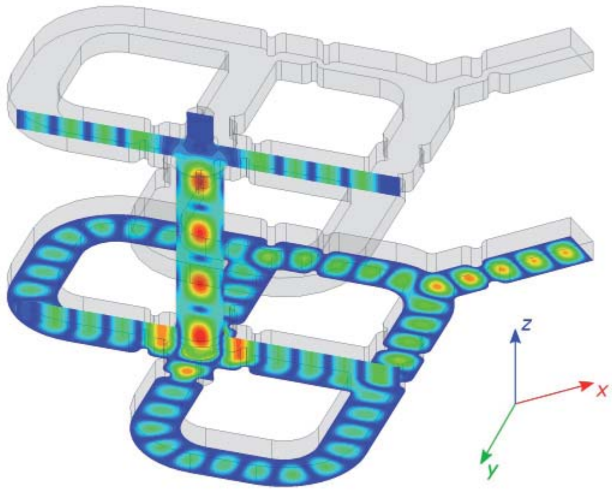

Figure 1. A three-dimensional model of the back-to-back structure. The simulated electric field of the two mode launcher arms as well as the central circular waveguide section are visible.

launchers joined through a central circular waveguide. This back-to-back configuration allowed us to characterize the structure in terms of *S* parameters, and also permitted measuring the electric field along the circular waveguide axis and along the azimuthal coordinate at a fixed radius through the bead-pull technique.

2. Mode Launcher RF Design

The presented mode launcher, working at X band, uses four symmetric sidewall coupling apertures of proper dimensions that, being fed with equal amplitude in-phase signals, excite the TM_{01} mode. The geometry of the branching network reduces the overall structure dimensions and allows the on-axis power coupling of the azimuthally symmetric accelerating mode. Thanks to the previously mentioned fourfold symmetry, the structure is able to minimize the undesired quadrupole modes [6]. Figure 1 shows the three-dimensional model of the structure in back-to-back configuration: the two mode-launcher sections with fourfold symmetry and the central circular waveguide with the TM_{01} mode are visible.

2.1 Mode-Launcher Feeding Layout Design

Details on the TM_{01} mode-launcher feeding layout, the delay line to match the phase at the sidewall coupling apertures, and matching bumps can be found in [7]. The H-plane branching network was optimized with a quasi-two-dimensional model [5] that took advantage of the field-translational symmetry to use a reduced computational domain. The TE_{10} rectangular waveguide branching line, shown in Figure 1, was studied taking advantage of the y invariance of the TE_{10}-mode fields. This allowed very fast two-dimensional simulation compared to a full-wave three-dimensional model. However, two-dimensional models (except for the case of ideal PEC waveguides) fail to correctly evaluate the waveguide losses. It is possible to restore the correct attenuation by introducing a fictitious conductivity, σ', for the top/bottom a-wide side of the waveguide:

$$\sigma' = CF\sigma = \left(\frac{b}{b'}\right)^2 \sigma , \tag{1}$$

where the correction factor $CF = \left(b/b'\right)^2$, is given by the ratio between the initial three-dimensional height, b, and the reduced height, b', of the quasi-two-dimensional model. Thanks to the correction factor on the top/bottom waveguide walls of the reduced b' height model, the correct attenuation loss can be accurately predicted.

The correction introduced above is valid for H-plane devices supporting TE_{p0} modes. However, to the extent the waveguide height, b, is kept low, higher TE_{pq} with $q \neq 0$ are not supported by the structure. Standard waveguide devices usually fulfill this requirement.

By taking advantage of the fast simulations, the branching network of Figure 1 was optimized. After the optimization, full-height three-dimensional simulations were carried out to model the side coupling in the four rectangular-to-circular side-aperture transitions.

2.2 Computation of Multipole Component Coefficients

The accelerating voltage inside the circular waveguide can be expressed as [7]

$$V_{\pm} = \int_{z_0}^{z_f} E_z\left(r,\theta,z\right) e^{\pm i k_0 z} dz , \tag{2}$$

Table 1. The discrete Fourier coefficients for the presented fourfold device compared to the simulated single and dual port devices

	Single Port	Dual Port	Quad Port
M_0	23.25	21.30	21.05
M_1	0.266	1.923×10^{-4}	2×10^{-3}
M_2	0.0714	0.0925	2.697×10^{-4}

where r, θ, and z are respectively the radial, azimuthal, and axial coordinates of the circular waveguide section. k_0 is the wavenumber of the RF input power, and z_0, z_f are the starting and the ending points of the linear path through which the axial voltage is being integrated.

The multipole components of the structure were calculated through the discrete Fourier transform of the accelerating voltage, given by [4]

$$M_{\pm,s}\left(r\right)=\frac{1}{\sqrt{n}}\sum_{j=1}^{n}V_{\pm}\left(r,\theta_j\right)e^{2\pi i(j-1)s/n}, \qquad (3)$$

where n is the number of the calculated azimuthal variations, $M_{\pm,s}$ is the calculated mode with index s (M_0 for monopolar, M_1 for dipolar, M_2 for quadrupolar component).

In order to verify the minimization of the quadrupole components obtained with the presented structure, two other mode-launching structures operating at 11.424 GHz were simulated, in back-to-back configuration, in Ansys *HFSS*. These are not reported here for the sake of brevity. One was a device that converts the TE_{10} into the TM_{01} by using a single rectangular waveguide. The other was a device that converts the TE_{10} into the TM_{01} by using two rectangular waveguides. Table 1 reports the discrete Fourier coefficients, calculated through Equation (3), for the three devices discussed and with the following parameters:

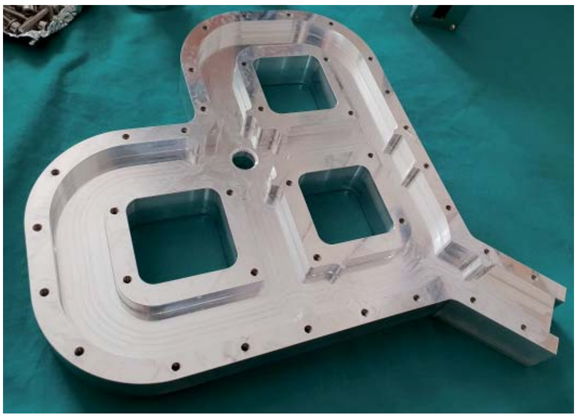

Figure 2a. A photo of the manufactured aluminum mode launcher for low-power-RF tests: the slotted plane of the mode launcher.

$r = 4$ mm, $\theta \in [0;360]$ degrees, $z_f - z_0 = 88$ mm (i.e., the total length of the circular waveguide section comprising the thickness of the aluminum walls).

From Table 1, it can be seen that the structure presented minimized the quadrupolar component of about two orders of magnitude with respect to the simulated single and dual-port structures.

3. Fabrication and Low-Power-Microwave Tests

Figures 2a and 2b respectively show an internal view of the mode-launcher structure and the final assembled identical mode launchers. The figures also show the central junction on which the circular waveguide section was connected.

The mode-launcher structure was composed of two aluminum halves: a milled plate where the waveguide branching was machined (see Figure 2a) and a plane cover that closed the assembly. The milling of aluminum blocks was done using a tolerance of 10 μm and a surface roughness of 100 nm. Because the "low-power-microwave test" aluminum structure was based on two pieces, it required a large number of screws, properly positioned in order to ensure good RF contact between the two parts.

Two identical aluminum prototypes (Figure 2b) were fabricated in order to perform the experimental RF characterization. These two prototypes were joined together through a 62 mm-long circular waveguide.

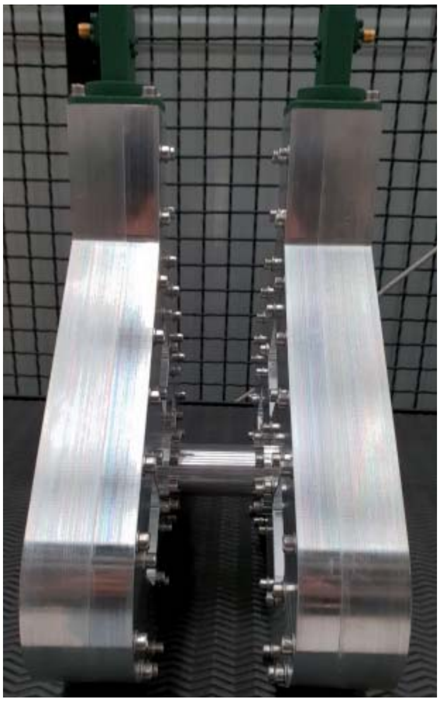

Figure 2b. Photos of two identical fabricated mode launchers for the back-to-back measurement.

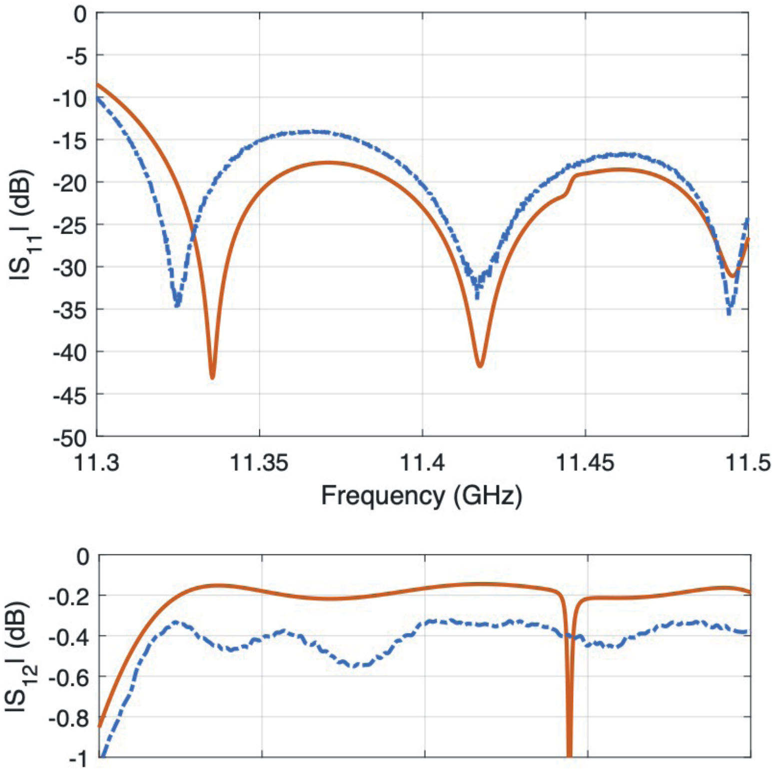

Figure 3. A comparison of the measured (blue dash-dotted curve) and simulated (orange curve) reflection and transmission coefficients, $|S_{11}|$ and $|S_{12}|$, for the full device in back-to-back configuration. At the working frequency of 11.42 GHz, the measured $|S_{11}|$ was about -30 dB while the $|S_{12}|$ was about -0.3 dB.

3.1 Measurement of *S* Parameters

A vector network analyzer was connected to the input and output rectangular waveguide sections of the full structure. Figure 3 shows the comparison between the simulated and experimental scattering parameters $|S_{11}|$ and $|S_{12}|$, respectively) of the assembled prototype.

The device was well matched into the interval of 11.3 GHz to 11.5 GHz: at the operating frequency of 11.42 GHz, the measured $|S_{11}|$ had values below -30 dB, while the measured $|S_{12}|$ was about -0.3 dB. A back-to-back measurement showed that the averaged loss of the mode launcher was about 0.2 dB higher than the value predicted by the simulation. This was likely due to the losses resulting from imperfect electrical contact in this non-brazed low-power-microwave test prototype.

3.2 Measurement of Electric Field Through Nonresonant Perturbation Technique

The electric field of the structure was measured through the use of the bead-pull technique. The adopted technique made use of the Steele non-resonant perturbation theory [3], employable when the measurement was performed on a traveling-wave structure such that presented in this paper. In the bead-pull technique, a small (in our case, dielectric) bead, attached to a nonconductive wire, was moved along the structure (in our case, along the waveguide axis), and the S_{11p} value was acquired at each sampled point. The electric field was proportional to the quantity $\Delta S_{11} = S_{11p} - S_{11np}$, where S_{11np} is the unperturbed value, i.e., the value when the bead was outside of the structure. When using the Steele theorem for the field measurement, the values at each sample point were acquired at a fixed frequency. In our case, we performed the measurements at the main resonant frequency, that is, 11.42 GHz.

A sketch of the experimental setup used for the bead-pull measurements is shown in Figure 4a. It was composed of a main metallic plate that held the stepping motor, necessary for the movement of the dielectric wire, and the device under test. A weight was attached at the wire end in order to maintain its tension.

Figure 4b shows a photo of the experimental setup. We used a two-port Agilent N5230A PNA-L microwave network analyzer that was interfaced to the stepping motor through a *LabView* script, able to command the wire movement as well as the sample rate. For the axial field measurement, an interval of 100 mm was chosen, with a sampling rate of 1 mm. The starting point was chosen at the circular waveguide's cutoff aperture. We chose a bead made of glue with a diameter of $\simeq 1$ mm as the perturbing object.

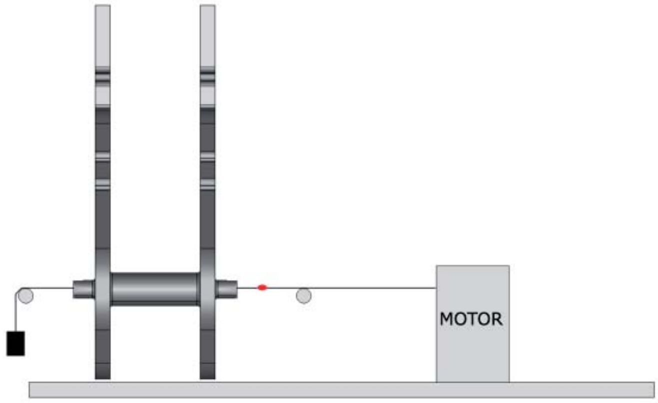

Figure 4a. A sketch of the bead-pull setup on the mode launcher. The perturbing dielectric bead is shown in red.

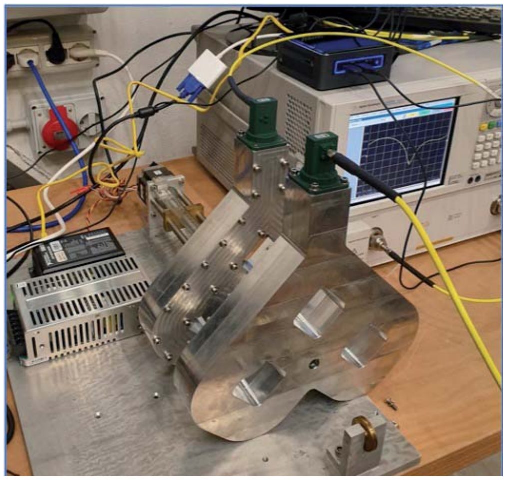

Figure 4b. A photograph of the bead-pull setup used for the E-field measurements on the mode launcher circular waveguide longitudinal axis.

Figure 5 shows the axial measurement of $\Delta|S_{11}|$ as a function of bead position performed on the device in back-to-back configuration, and the corresponding electric field *HFSS* simulation. Both curves were normalized with respect to their maxima. The two curves resulted in good agreement with each other.

The $\Delta|S_{11}|$ values were also measured inside the circular waveguide, along a circumference of radius $r = 4$ mm at the axial position $z = 90$ mm (i.e., at a position of electric-field maximum). For the azimuthal $|S_{11}|$ measurement, a circular flange was employed. The flange was rotated with a 10° step and a constant $\Delta|S_{11}|$ was measured. This further confirmed the field symmetry and the absence of competing quadrupolar modes.

4. Conclusion

A novel RF power coupler for an RF photoinjector, designed for high-brightness applications, has been presented. The design was partially automated by taking advantage of an ad hoc developed two-dimensional model with reduced simulation time. The proposed mode launcher was an X-band TM_{01} waveguide mode launcher that minimized dipole and quadrupole field components. A low-power-microwave version of the mode launcher was fabricated and successfully tested. This launcher features good back-to-back performance. We plan to test a brazed version of this mode launcher for a high-power test at SLAC.

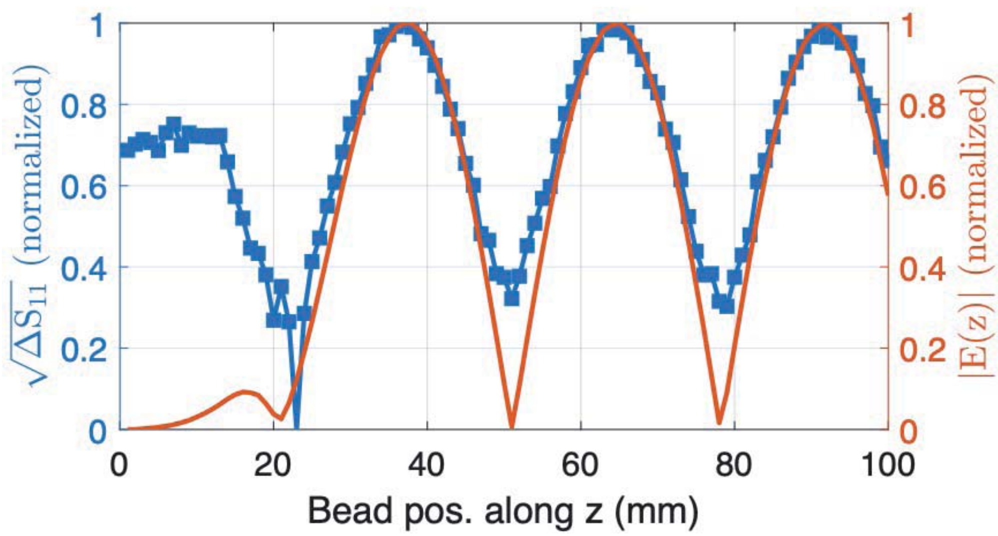

Figure 5. The measured $|S_{11}|$ values as a function of bead position (blue curves) and a comparison with the *HFSS* electric-field simulations (red curves).

5. References

1. D. Alesini et al., "Design of High Gradient, High Repetition Rate Damped C-Band RF Structures," *Phys. Rev. Accel. Beams*, **20**, March 2017, p. 032004.

2. A. D. Cahill, J. B. Rosenzweig, V. A. Dolgashev, S. G. Tantawi, and S. Weathersby, "High Gradient Experiments with X-Band Cryogenic Copper Accelerating Cavities," *Phys. Rev. Accel. Beams*, **21**, October 2018, p. 102002.

3. C. W. Steele, "A Nonresonant Perturbation Theory," *IEEE Trans. Microw. Theory Techn.*, **14**, February 1966, pp. 70-74.

4. A. Cahill, M. Dal Forno, and V. A. Dolgashev, "TM01 Mode Launcher for Use in High Brightness Photoguns," 7th International Particle Accelerator Conference, IPAC16, 2016, pp. 491-493.

5. G. Castorina, G. Torrisi, G. Sorbello, L. Celona, and A. Mostacci, "Conductor Losses Calculation in Two-Dimensional Simulations of H-Plane Rectangular Waveguides," *J. of Electromagnet. Wave*, 2019, pp. 1-10.

6. T.-H. Chang, C.-H. Li, C.-N. Wu, and C.-F. Yu, "Generating Pure Circular TE_{mn} Modes Using Y-Type Power Dividers," *IEEE Trans. Microw. Theory Techn.*, **58**, 6, 2010, pp. 1543-1550.

7. G. Castorina et al., "TM_{01} Mode Launcher with Quadrupole Field Components Cancellation for High Brightness Applications," *J. Phys.: Conf. Ser.*, 2018, p. 1067 082025.

James Clerk Maxwell Foundation *Newsletter* Available

The Winter 2020 edition of the *Newsletter* of the James Clerk Maxwell Foundation is available for free download at http://www.clerkmaxwellfoundation.org/Newsletter_2020_Winter.pdf. This edition contains an article by T. G. Mackay, "New Electromagnetic Waves: Voigt Surface Waves."